

# Nonstationary pattern in unsynchronizable complex networks

Xingang Wang,<sup>1,2</sup> Meng Zhan,<sup>3</sup> Shuguang Guan,<sup>1,2</sup> and Choy Heng Lai<sup>4,2</sup>

<sup>1</sup>*Temasek Laboratories, National University of Singapore, 117508 Singapore*

<sup>2</sup>*Beijing-Hong Kong-Singapore Joint Centre for Nonlinear & Complex Systems (Singapore),  
National University of Singapore, Kent Ridge, 119260 Singapore*

<sup>3</sup>*Wuhan Institute of Physics and Mathematics, Chinese Academy of Sciences, Wuhan 430071, China*

<sup>4</sup>*Department of Physics, National University of Singapore, 117542 Singapore*

(Dated: November 12, 2018)

Pattern formation and evolution in unsynchronizable complex networks are investigated. Due to the asymmetric topology, the synchronous patterns formed in complex networks are irregular and nonstationary. For coupling strength immediately out of the synchronizable region, the typical phenomenon is the on-off intermittency of the system dynamics. The patterns appeared in this process are signatored by the coexistence of a giant cluster, which comprises most of the nodes, and a few number of small clusters. The pattern evolution is characterized by the giant cluster irregularly absorbs or emits the small clusters. As the coupling strength leaves away from the synchronization bifurcation point, the giant cluster is gradually dissolved into a number of small clusters, and the system dynamics is characterized by the integration and separation of the small clusters. Dynamical mechanisms and statistical properties of the nonstationary pattern evolution are analyzed and conducted, and some scalings are newly revealed. Remarkably, it is found that the few active nodes, which escape from the giant cluster with a high frequency, are independent of the coupling strength while are sensitive to the bifurcation types. We hope our findings about nonstationary pattern could give additional understandings to the dynamics of complex systems and have implications to some real problems where systems maintain their normal functions only in the unsynchronizable state.

PACS numbers: 89.75.-k, 05.45.Xt

## I. INTRODUCTION

Synchronization of complex networks has aroused many interest in nonlinear science since the discoveries of the small-world and scale-free properties in many real and man-made systems [1, 2]. In this study, one important issue is to explore the inter-dependent relationship between the collective behaviors of the complex systems and their underlying topologies. In particular, many efforts have been paid to the construction of optimal networks, and a number of factors which have important affections to the synchronizability of complex networks have been gradually disclosed. Now it is known that random networks, due to their small average distances, are generally more synchronizable than regular networks [3, 4]; and scale-free networks, with weighted and asymmetric couplings, can be more synchronizable than homogeneous networks [5, 6]. In these studies, the standard method employed for synchronization analysis is the master stability function (MSF), where the network synchronizability is estimated by an eigenratio calculated from the coupling matrix, and system which has a smaller eigenratio is believed to be more synchronizable than that of larger eigenratio [7]. Inspired by this, to improve the network synchronizability, the only task seems to be upgrading the coupling matrix so as to decrease the eigenratio, either by changing the network topology [4] or by adjusting the coupling scheme [5, 6].

The MSF method, while bringing great convenience to the analysis, overlooks the temporal, local property of the system and reflects only partial information about the system dynamics. Specifically, from MSF we only know ultimately whether the network is globally synchronizable or unsynchronizable, but do not know how the global synchronization is

reached if the network is synchronizable, or what's the pattern and how it evolves if the network is unsynchronizable. These evolution details, or the transient behavior in system development, contain rich information about the system dynamics and may give additional insights to the organization of complex systems. For instance, the recent studies about synchronization transition have shown that, in the unsynchronizable states, heterogeneous networks are more synchronizable (have a higher degree of coherence) than homogeneous networks at small couplings, while at larger couplings the opposite happens [8]. This crossover phenomenon of network synchronizability are difficult to understood if we only look at the final state of the system, but are straightforward if we look at the transient behaviors of their evolutions [8]. Besides revealing the synchronization mechanisms, the transient behavior of network synchronization can also be used to detect the topological scales and hierarchical structures in the real systems, e.g., the detection of cluster structures in social and biological networks [9, 10]. However, despite of its theoretical and practical significance, the study of transient dynamics of complex networks is still at its infancy and many questions remain open, say for example, the pattern evolution of unsynchronizable complex networks.

Pattern formation in unsynchronizable but near-synchronization networks has been an important issue in studying the collective behavior of regular networks [11, 12]. By setting the coupling strength nearby the synchronization bifurcation point, the system state shares both the dynamical properties of the synchronizable and unsynchronizable states: a state of high coherence but is not synchronized. The bifacial dynamical property makes this state a natural choice in investigating the transition process of networks synchronization. Previously studies about regular

networks, say for example the lattices [11], have shown that, when the coupling strength is slightly out of the synchronizable region, although global synchronization is unreachable, nodes are still synchronized in a partial sense. That is, nodes are self-organized into a number of synchronous clusters. The distribution of these clusters, also called the synchronous pattern, is determined by a set of factors such as the coupling strength, the system size and the coupling scheme. As the coupling strength leaves away from the bifurcation point, the pattern structure becomes more and more complicated and the system coherence will be decreased, and finally reaches the turbulence state. It is worthy of note that the patterns arisen in regular networks have two common properties: spatially symmetric and temporally stationary. More specifically, the contents of each cluster are fixed and the clusters are of translation symmetry in space. For this reason, we say that *the patterns formed in regular networks are symmetric and stationary*. These two properties, as have been discussed in the previous studies [11, 12], are rooted in the symmetric topology of the regular networks. This makes it interesting to ask the following question: how about the patterns in unsynchronizable complex networks?

Different to the regular networks, in complex networks we are not able to find any symmetry from their topologies. The asymmetric topology, according to the pattern analysis developed in studying regular networks [11], will induce two significant changes to the patterns: 1) the synchronous clusters, if they exist, will be asymmetric; and 2) all the possible patterns, including the one of global synchronization, are linearly unstable under small perturbations. In other words, *the patterns formed in complex networks are expected to be asymmetric and nonstationary*. Our mission of this paper is just to understand and characterize the nonstationary patterns arisen in the development of complex networks. Specifically, we are trying to investigate the following questions: 1) is there any pattern arises during the system evolution? 2) the pattern is stationary or nonstationary? if nonstationary, how is it evolving and how is it reflected from the system dynamics? 3) What happens to the pattern properties during the transition of network synchronization? and 4) How the coupling strength and bifurcation type affect the pattern properties? By investigating these dynamical and statistical properties, we wish to have a global understanding to the dynamics of unsynchronizable complex networks.

Our main findings are: 1) for coupling strength immediately outside of the synchronizable region, the system dynamics undergoes the process of on-off intermittency. That is, most of the time the system stays on the global synchronization state (the "off" state) but, once in a while, it develops into a breaking state (the "on" state) which is composed by a giant cluster and a few number of small clusters (hereafter we call it the giant-cluster state). As the system develops, the giant cluster changes its shape by absorbing or emitting the small clusters, leading to the "off" or "on" states, respectively; 2) the few active nodes which escape from the giant cluster with the high frequencies are coupling-strength independent but are bifurcation-type dependent. That is, in the neighboring region of a fixed bifurcation point, the locations

of these active nodes do not change with the coupling strength; if we change the coupling strength from nearby another bifurcation point (the two bifurcation points will be explained later), their locations will be totally changed; 3) as coupling strength leaves away from the bifurcation point, the giant cluster is gradually dissolved and more small clusters are generated from it. Eventually, the giant cluster disappears and the pattern is composed by only the small clusters (hereafter we call it the scattering-cluster state). During the course of system evolution, each small cluster may either increase its size by integrating with other small clusters or decrease its size by breaking to even small clusters, but it can never reach to the global synchronization state; 4) besides the giant cluster, the giant- and scattering-cluster states are also distinct in their small clusters. For giant-cluster state the size of the small clusters follows a power-law distribution, while for scattering-cluster state it follows a Gaussian distribution.

The rest of the paper is going to be arranged as follows. In Sec. II we will give our model of coupled map network and, based on the method of MSF, point out the two bifurcation points and the transition areas that we are going to study with. In Sec. III we will employ the method of finite-time Lyapunov exponent to predict and describe the intermittent system dynamics in the bifurcation regions. Direct simulations about on-off intermittency will be presented in Sec. IV. By introducing the method of temporal phase synchronization, in Sec. V we will investigate in detail the dynamical and statistical properties of the nonstationary pattern. Meanwhile, properties of the giant- and scattering states will be compared and the transition between the two states will be conducted. In Sec. VI we will discuss the phenomenon of active nodes and investigate their dependence to the network properties. Discussions and conclusions about pattern evolution in complex networks will be presented in Sec. VII.

## II. COUPLED MAP NETWORKS AND THE TWO BIFURCATION POINTS

Our model of coupled map network is of the following form

$$\mathbf{x}_i(t+1) = \mathbf{F}(\mathbf{x}_i(t)) - \varepsilon \sum_j G_{i,j} \mathbf{H}[\mathbf{f}(\mathbf{x}_j(t))]. \quad (1)$$

where  $\mathbf{x}_i(t+1) = \mathbf{F}(\mathbf{x}_i(t))$  is a  $d$ -dimensional map representing the local dynamics on node  $i$ ,  $\varepsilon$  is a global coupling parameter,  $G$  is Laplacian matrix representing the couplings, and  $\mathbf{H}$  is a coupling function. To facilitate our analysis, we adopt the following coupling scheme [13]:

$$G_{i,j} = -\frac{A_{i,j}k_j^\beta}{\sum_{j=1}^N A_{i,j}k_j^\beta}, \quad (2)$$

for  $j \neq i$  and  $G_{i,i} = 1$ , with  $k_i$  the degree of node  $i$  and  $A$  the adjacent matrix of the network:  $A_{i,j} = 1$  if node  $i$  and  $j$  are connected and  $A_{i,j} = 0$  otherwise. In comparison with the traditional coupling schemes, one important advantage we benefit from this coupling scheme is that the synchronizability of the network, i.e. the eigenratio of the coupling matrix

described in Eq. [2], can be easily adjusted by the parameter  $\beta$ , while the network topology is kept unchanged. This advantage brings many convenience in network selection since for a given network topology, even though it is unsynchronizable under the traditional schemes, can now be synchronizable by adjusting  $\beta$  in Eq. [2]. This convenience is of particular importance when our studies of network dynamics are focused on the bifurcation regions, where the network synchronizability should be deliberately arranged in order to demonstrate both the two types of bifurcations. We note that the adoption of Eq. [2] is only for the purpose of convenient analysis, the findings we are going to report are general and can also be observed by other coupling schemes given the network is properly prepared. In practice, we use logistic map  $\mathbf{F}(x) = 4x(1-x)$  as the local dynamics and adopt  $\mathbf{H}(\mathbf{x}) = x$  as the coupling function.

We first locate the two bifurcation points of global synchronization. The linear stability of the global synchronization state  $\{x_i(t) = s(t), \forall i\}$  is determined by the corresponding variational equations, which can be diagonalized into  $N$  blocks of form

$$y(t+1) = [\mathbf{DF}(s) + \sigma \mathbf{DH}(s)] y(t), \quad (3)$$

with  $\mathbf{DF}(s)$  and  $\mathbf{DH}(s)$  the Jacobian matrices of the corresponding vector functions evaluated at  $s(t)$ , and  $y$  represents the different modes that are transverse to the synchronous manifold  $s(t)$ . We have  $\sigma(i) = \varepsilon \lambda_i$  for the  $i$ th block,  $i = 1, 2, \dots, N$ , and  $\lambda_1 = 0 \leq \lambda_2 \leq \dots \leq \lambda_N$  are the eigenvalues of matrix  $G$ . The largest Lyapunov exponent  $\Lambda(\sigma)$  of Eq. [3], known as the master stability function (MSF) [7], determines the linear stability of the synchronous manifold  $s(t)$ . In particular, the synchronous manifold is stable if only  $\Lambda(\varepsilon \lambda_i) < 0$  for each  $i = 2, \dots, N$ . The set of Lyapunov exponents  $\Lambda(\varepsilon \lambda_i)$  govern the stability of the synchronous manifold in the transverse spaces, and a positive value of  $\Lambda(\varepsilon \lambda_i)$  represents the loss of the stability in the transverse space of mode  $i$ . It was found that for a large class of chaotic systems,  $\Lambda(\sigma) < 0$  is only fulfilled within a limit range in the parameter space  $\sigma \in (\sigma_1, \sigma_2)$ . This indicates that, to make the global synchronization state linearly stable, all the eigenvalues  $\lambda_i$  should be contained within range  $(\sigma_1, \sigma_2)$ , i.e.,  $\lambda_N/\lambda_2 < \sigma_2/\sigma_1$ . For the logistic map employed here, it is not difficult to prove that  $\sigma_1 = 0.5$  and  $\sigma_2 = 1.5$ . Therefore, to achieve global synchronization, the coupling matrix  $G$  should be designed with eigenratio  $R \equiv \lambda_N/\lambda_2 < \sigma_2/\sigma_1 = 3 = R_c$ .

Besides the condition of  $R < R_c$ , to guarantee the synchronization, we also need to set the coupling strength in a proper way: either small or large couplings may deteriorate the synchronization. If  $\varepsilon < \varepsilon_1 = \sigma_1/\lambda_2$ , the couplings are too weak to restrict the node trajectories to the synchronous manifold; while if  $\varepsilon > \varepsilon_2 = \sigma_2/\lambda_N$ , the couplings will be too strong and actually act as large perturbations to the synchronization manifold. Therefore, to achieve the global synchronization, we also require  $\varepsilon_1 < \varepsilon < \varepsilon_2$ . The two critical couplings  $\varepsilon_1$  and  $\varepsilon_2$ , which are named as the long-wave (LW) [14] and short-wave (SW) bifurcations [15] respectively in the studies of regular networks, thus stand as the boundaries of the synchronizable region. Our studies about network synchroniza-

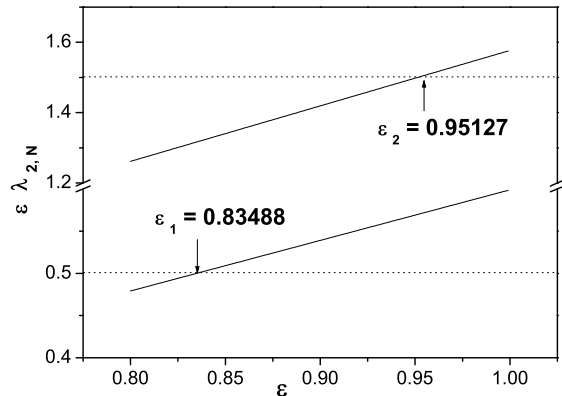


FIG. 1: For scale-free network of  $N = 1000$  nodes and of average degree  $\langle k \rangle = 8$ , a schematic plot on the generation of the two bifurcation points as a function of the coupling strength. The long-wave bifurcation occurs at about  $\varepsilon_1 \approx 0.83488$  which is determined by the condition  $\varepsilon \lambda_2 = \sigma_1 = 0.5$  (the lower line). The short-wave bifurcation occurs at about  $\varepsilon_2 \approx 0.95127$  which is determined by the condition  $\varepsilon \lambda_N = \sigma_2 = 1.5$  (the upper line).

tion will be focused on the neighboring regions of the two bifurcation points, i.e., the region of  $\varepsilon \lesssim \varepsilon_1$  or  $\varepsilon \gtrsim \varepsilon_2$ .

By the standard BA growth model [1], we construct a scale-free network of  $10^3$  nodes and of average degree  $\langle k \rangle = 8$ . By setting  $\beta = 2.5$  in Eq. [2], we have  $\lambda_2 \approx 0.6$  and  $\lambda_N \approx 1.58$ . Because of  $R = \lambda_N/\lambda_2 \approx 2.6 < R_c$ , the network is globally synchronizable. Also, because of  $\lambda_2 > \sigma_1$  and  $\lambda_N > \sigma_2$ , both the two bifurcations can be realized by adjusting the coupling strength within range  $\varepsilon \in (0, 1)$ . In specific, when  $\varepsilon < \varepsilon_1 \approx 0.835$ , we have  $\varepsilon \lambda_2 < \sigma_1$  and  $\varepsilon \lambda_N < \sigma_2$ , the synchronous manifold loses its stability at the lower boundary of the synchronizable region and LW bifurcation occurs; and when  $\varepsilon > \varepsilon_2 \approx 0.95$ , we have  $\varepsilon \lambda_2 > \sigma_1$  and  $\varepsilon \lambda_N > \sigma_2$ , the synchronous manifold loses its stability at the upper boundary of the synchronizable region and SW bifurcation occurs [Fig. 1]. In the following we will fix the network topology and the parameter  $\beta$ , while generating the various patterns by changing the coupling strength  $\varepsilon$  nearby the two bifurcation points.

### III. FINITE-TIME LYAPUNOV EXPONENT

Before direct simulations, we first give a qualitative description (prediction) on the possible system dynamics in bifurcation regions. To concrete our analysis, in the following we will only discuss the situation of SW bifurcation ( $\varepsilon \lesssim \varepsilon_1$ ), while noting that the same phenomena can be found at the LW bifurcation as well ( $\varepsilon \gtrsim \varepsilon_2$ ). In preparing the unsynchronizable states, we only let  $\Lambda(\lambda_2)$  be slightly puncturing into the unstable region, while keeping all the other exponents still staying in the stable region, i.e.,  $\Lambda(\lambda_2) \gtrsim 0$  and  $\Lambda(\lambda_i) < 0$  for  $i = 3, \dots, N$ . With this setting, the synchronous manifold is only desynchronized in the transverse space of mode 2. As

such, the system possesses only two positive Lyapunov exponents, one is  $\Lambda(\lambda_0)$  which is associated to the synchronous manifold itself and another one is  $\Lambda(\lambda_2)$ . Noticing that  $\Lambda(\lambda)$  are asymptotic averages, and, as so, they account only for the global stability properties, but do not warrant the possible coherent sets arising in the system evolutions. These coherent sets, for regular networks, refer to the stationary, symmetric patterns to which the system finally develops. While for complex networks, these sets can be the temporal, irregular clusters emerged in the process of system evolution.

In the region of  $\varepsilon \lesssim \varepsilon_1$ , although global synchronization is unreachable, the system may still keep with the high coherence due to the existence of the synchronous clusters. Especially, there could be some moments at which all the trajectories are restrained to a small region in the phase space, very close to the situation of global synchronization. This varying system coherence, however, can not be reflected from the asymptotic value  $\Lambda(\lambda)$ . To characterize the variation, we need to employ some new quantities which are able to capture the temporal behavior of system. One of such quantities is the finite-time Lyapunov exponent (FLE), a technique developed in studying chaos transition in nonlinear science [16]. In stead of asymptotic average, FLE measures the diverging rate of nearby trajectories only in a finite time interval  $T$ .

$$\Lambda_i = \frac{1}{T} \sum_{t=(i-1)T}^{iT} \ln \mathbf{DH}(s(t)). \quad (4)$$

As our studies are focused on the situation of one-mode desynchronization, the stability of the synchronous manifold and the temporal behavior that it displays are therefore expected to be more reflected from the variation of  $\Lambda_{2,i}$ , the FLE that associates with mode 2. With  $\varepsilon = 0.83$  and  $T = 100$ , we plot in Fig. 2 the time evolution of  $\Lambda_{2,i}$ . It is found that, although with a positive asymptotic value about  $\langle \Lambda_{2,i} \rangle \approx 6 \times 10^{-3}$ , the instant value of  $\Lambda_{2,i}$  penetrates to the negative region at a high frequency. According to the different signs of  $\Lambda_{2,i}$ , the system evolution is divided into two types of intervals: the divergent interval and the contractive interval. In the divergent intervals we have  $\Lambda_{2,i} > 0$  and the system dynamics is temporarily dominated by the divergence of the node trajectories from the synchronous manifold; while in the contractive intervals we have  $\Lambda_{2,i} < 0$  and the system dynamics is temporarily dominated by the convergence of the node trajectories to the synchronous manifold.

The variation of  $\Lambda_{2,i}$ , reflected on the process of pattern evolution, characterizes the travelling property of the system dynamics among the neighboring regions of two different kinds of states: the desynchronization state and the synchronization state. In Fig. 2, the minimum value of  $\Lambda_{2,i}$  is about  $-0.07$ , during this contractive interval the node trajectories will converge to the synchronous manifold by an amount of  $e^{\min \Lambda_{2,i} T} \approx e^{-7} \approx 10^{-3}$  on average. Assuming that before entering this interval the average distance between the node trajectories is  $\Delta$  (for logistic map we always have  $\Delta < 1$ ), then at the end of this interval the average distance is decreased to  $\Delta \times 10^{-3}$ , a small value which is usually overshadowed by noise in practice. Due to this small distance,

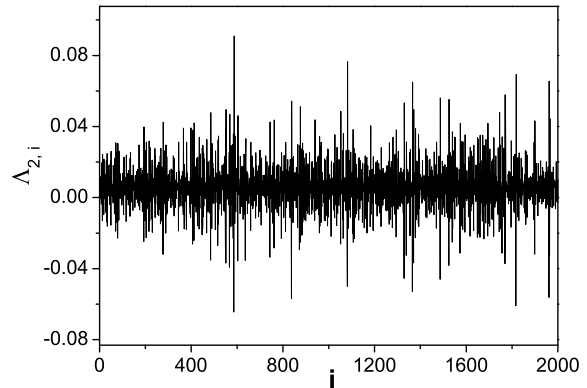


FIG. 2: For  $\varepsilon = 0.83$  in Fig. 1, the time evolution of the finite-time Lyapunov exponent  $\Lambda_{2,i}$  calculated on intervals of length  $T = 100$ . It is observed that, while having the positive asymptotic value  $\langle \Lambda_{2,i} \rangle > 0$ , the temporal value of  $\Lambda_{2,i}$  is penetrating into the negative region frequently.

the system can be practically regarded as already reached the synchronization state. On the other hand, if the system enters a divergent interval, the node trajectories will diverge from each other and, at the end of this interval, their average distance will be increased by an order of  $10^3$ . This large distance will deteriorate the ordered trajectories (or the high coherence of the system dynamics) that achieved during the contractive intervals, and leading to the incoherent, breaking state. The pattern of the breaking state, however, is not unique. Depending on the initial conditions and the divergence intervals, the pattern may assume the different configurations. Therefore, based on the observations of  $\Lambda_{2,i}$  [Fig. 2] the dynamics of unsynchronizable networks can be intuitively understood as an intermittent travelling among the synchronization state and the different kinds of desynchronization states.

#### IV. ON-OFF INTERMITTENCY DESCRIBED BY COMPLETE SYNCHRONIZATION

We now investigate the system dynamics by direct simulations. To implement, we first prepare the system to be staying on the synchronization state. This can be achieved by adopting a large coupling strength from the synchronizable region, i.e.  $\varepsilon_1 < \varepsilon < \varepsilon_2$ . After synchronization is achieved, we then decrease  $\varepsilon$  to a value slightly below the bifurcation point  $\varepsilon_1$  and, in the meantime, an instant small perturbation is added on each node. In practice, we take i.i.d (independent identically distributed) noise of strength  $1 \times 10^{-5}$  as the perturbations. After this, we release the system and let it develop according to Eq. (1). Since  $\varepsilon < \varepsilon_1$ , the synchronization state is unstable and, triggered by the noises, the node trajectories begin to diverge from each other. The divergent trajectories, however, will frequently visit the neighborhood of the synchronous manifold, especially during those contractive intervals of small  $\Lambda_{2,i}$  [Fig. 2]. The intermittent system dynamics

is plotted in Fig. 3(a), where the average trajectory distance  $\Delta X = \frac{1}{N} \sum_{i=1}^N x_i - \bar{x}$  is plotted as a function of time. As we have predicted from LLE, the system dynamics indeed undergoes an intermittent process. To characterize the intermittency, we plot in Fig. 3(b) the laminar-phase distribution of the  $\Delta X$  sequence plotted in Fig. 3(a). It is found that the laminar length  $\tau$  (the time interval between two adjacent bursts of amplitude  $\Delta X(t) > 10^{-3}$ ) and the probability  $p(\tau)$  for it to appear follow a power-law scaling  $p(\tau) \sim \tau^{-\gamma}$ . The fitted exponent is about  $\gamma \approx -1.5 \pm 0.05$ , with a fat tail at large  $\tau$  due to the finite simulating time.

In chaos theory, intermittent process of laminar-phase exponent  $-3/2$  is classified as the "on-off" intermittency, a typical phenomenon observed in dynamical systems with a symmetric invariant set [17]. On-off intermittency is also reported in chaos synchronization of regular networks, where the invariant set refers to the synchronous manifold, and the "off" state refers to the long stretches that the system dynamics is staying nearby the synchronous manifold and the "on" state refers to the short bursts that the system dynamics is staying away from the synchronous manifold. Therefore, in terms of laminar-phase distribution, the intermittency we have found in complex networks [Fig. 3] has no difference to the that of the regular networks, despite of the drastic difference between their topologies. We have also investigated the transition behavior of the averaged distance  $\langle \Delta X(t) \rangle$  nearby the bifurcation points. As shown in Fig. 3(c), a linear relation between  $\langle \Delta X(t) \rangle$  and  $\varepsilon$  is found in the region of  $\varepsilon \lesssim \varepsilon_1$ . This linear transition of the system performance, again, is consistent with the transition of regular networks [18]. Therefore, in terms of complete synchronization, the on-off intermittency we have found in complex networks has no difference to that of the regular networks.

## V. PATTERN EVOLUTION IN COMPLEX NETWORKS

To reveal the unique properties of the system dynamics that induced by the complex topology, we go on to investigate the pattern formation of unsynchronizable networks by the method of temporal phase synchronization (TPS).

### A. Temporal phase synchronization

TPS is defined as follows. Let  $x_i(t)$  be the time sequence recorded on node  $i$ , we first transform it into a symbolic sequence  $\theta_i(t)$  according to the following equations

$$\theta_i(t) = \begin{cases} 0, & \text{if } x_i(t) < 0.5, \\ 1, & \text{if } x_i(t) \geq 0.5. \end{cases} \quad (5)$$

Then we divide  $\theta_i(t)$  into short segments of the equal length  $n$ . Regarding each segment as an new element, we therefore have transformed the long, variable sequence  $x_i(t)$  into a short, symbolic sequence  $\Theta_i(t')$ . If at moment  $t'$  we have  $\Theta_i(t') = \Theta_j(t')$ , then we say that TPS is achieved between

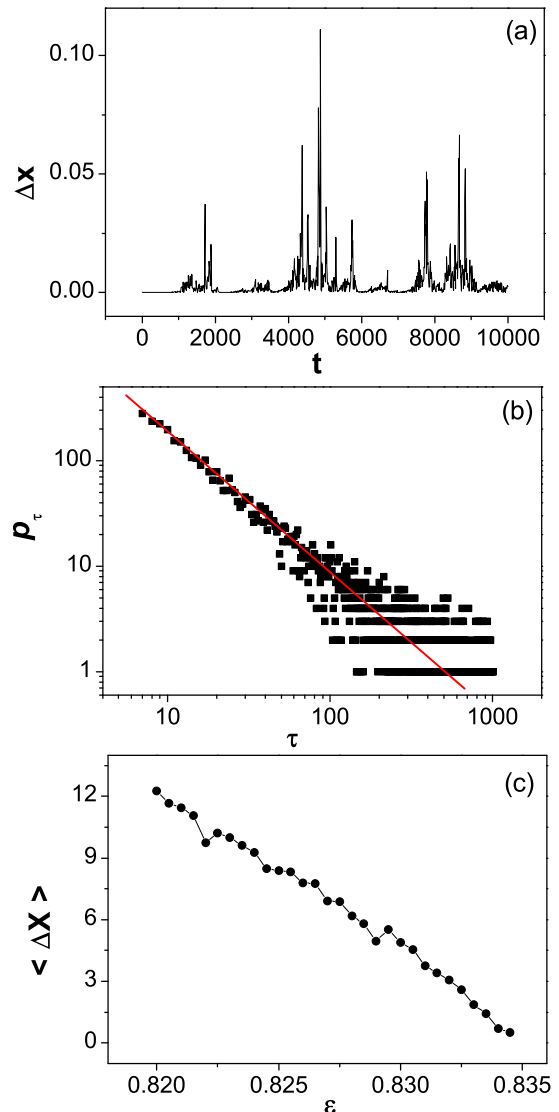


FIG. 3: (Color online) The on-off intermittency of the system dynamics nearby the LW bifurcation at  $\varepsilon = 0.83$ . (a) The time evolution of the average trajectory distance  $\Delta X$ . (b) The laminar-phase distribution of  $\Delta X$ , which follows a power-law scaling with the fitted exponent around  $3/2$ . (c) The transition behavior of the average distance  $\langle \Delta X \rangle$  nearby the LW bifurcation point  $\varepsilon_1$ , where a linear relation is found between the two quantities.

the nodes  $i$  and  $j$ . The collection of nodes which have the same value of  $\Theta$  at moment  $t'$  are defined as a temporarily synchronous cluster, and all the synchronous clusters constitute the temporarily pattern of the system. During the course of system evolution, the clusters will change their shapes and contents and the pattern will change its configuration.

In comparison with the method of complete synchronization, the advantage we benefit from TPS is obvious: it makes the synchronous pattern detectable. With complete synchronization, it is almost impossible for two nodes to have ex-

actly the same variable at the same time. Despite the fact that at some moments the system has already reached the high-coherence states (formed during those contractive intervals in Fig. 3(a)), with complete synchronization we are not able to distinguish these states from those low-coherence ones quantitatively (formed during those divergent intervals in Fig. 3(a)). (A remedy to this difficulty seems to define the clusters by the method of threshold truncation, i.e., nodes are regarded as synchronized if the distance between their trajectories is smaller than some small value. However, this definition of synchronization will induce the problem of cluster identification, as the same state may generate different patterns if we choose the different reference nodes.) On the contrary, TPS focuses on the loose match (phase synchronization) between the node variables over a period of time. By requiring an exact match of the discrete variable  $\Theta$ , the synchronous pattern is uniquely defined; while by requiring the match of the long sequences of  $\theta$ , the "synchronous" nodes are guaranteed with a strong coherence.

### B. Pattern evolution of the giant-cluster state

With the same set of parameters as in Fig. 3(a), by the method of TPS we plot in Fig. 4 the time evolutions of two basic quantities of pattern evolution: the number of synchronous clusters  $n_c$  and the size of the largest cluster  $L_{\max}$ . It is found that, similar to the phenomenon in complete synchronization [Fig. 3(a)], on-off intermittency is also found in the TPS quantities  $n_c$  and  $L_{\max}$ . In Fig. 4(a) it is shown that most of the time the system is broken into only a few number of clusters,  $n_c = 2$  or  $3$ , while occasionally it is broken into a quite large number of clusters,  $10 < n_c < 50$ , or united to the synchronization state,  $n_c = 1$ . The intermittent pattern evolution is also reflected on the sequence of  $L_{\max}$  [Fig. 4(b)], where most of the time the size of the giant cluster is about  $L_{\max} \approx N$ , while occasionally it decreases to some small values of  $L_{\max} < N/2$ . As we have discussed previously, the main advantage we benefit from TPS is in identifying the clusters. This advantage is clearly shown in Figs. 4(a) and (b), where for any time instant the two quantities  $n_c$  and  $L_i$  are uniquely defined. Besides cluster identification, we also benefit from TPS in quantifying the synchronization degrees. In specific, the different coherence states shown in Fig. 3(a) now can be clearly quantified: high coherence states are those of smaller  $n_c$  or larger  $L_{\max}$ . Specially, the synchronization state now is unambiguously defined as the moments of  $n_c = 1$  in Fig. 4(a) or, equally, the moments of  $L_{\max} = N$  in Fig. 4(b).

We go on to investigate the pattern evolution by statistical analysis. The first statistic we are interested is the laminar-phase distribution of the synchronization state, i.e. the time intervals that  $n_c = 1$  in Fig. 4(a) or  $L_{\max} = N$  in Fig. 4(b). In its original definition, laminar phase refers to the time intervals  $\tau$  that all node trajectories stays within a small distance from the synchronous manifold, therefore the actual value of  $\tau$  is varying with the predefined threshold distance. This uncertainty is overcome in TPS. As shown in Fig. 4(a), in TPS

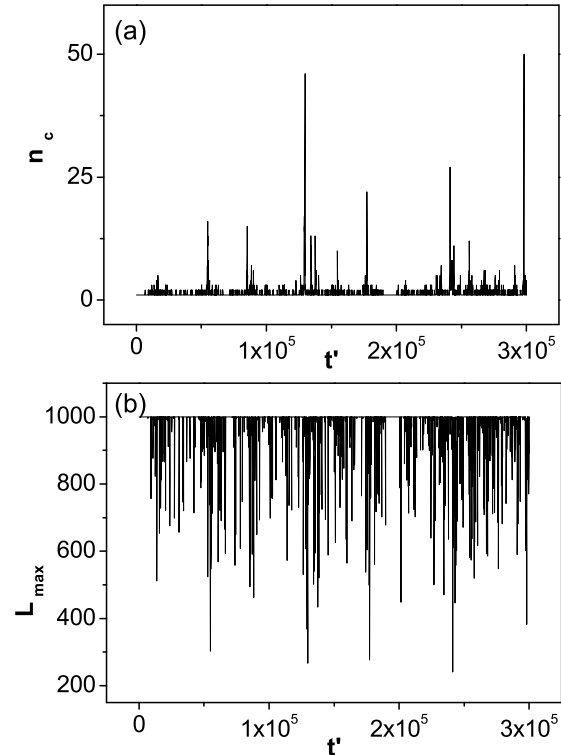


FIG. 4: For the same set of parameters as in Fig. 3(a). The time evolutions of the TPS quantities. (a) The number of the synchronous clusters  $n_c$  and (b) the size of the giant cluster  $L_{\max}$ . The synchronization state is defined as the moments  $n_c = 1$  in (a) or  $L_{\max} = N$  in (b).

the "off" state refers to the moments of  $n_c = 1$  specifically. The laminar-phase distribution of  $n_c$  is plotted in Fig. 5(a). In consistency with the distribution of complete synchronization [Fig. 3], the laminar-phase distribution of  $n_c$  also follows a power-law scaling and has the same exponent  $\gamma \approx -1.5 \pm 0.1$ . Therefore the use of TPS, while bringing convenience to the pattern analysis, still capture the basic properties of the on-off intermittency. The second statistic we are interested is the size distribution of the largest cluster, an important indicator for the coherence degree of the system. For the  $L_{\max}$  sequence plotted in Fig. 4(b), in Fig. 5(b) we plot the size distribution of  $L_{\max}$ . It is seen that the probability of finding large cluster  $L_{\max} \approx N$  is much higher than that of small cluster of  $L_{\max} < 500$ . In particular, the probability for finding clusters of  $L_{\max} > 990$  is about 20 percent and for  $L_{\max} > 990$  it is about 70 percent. Therefore, in the region of  $\varepsilon \lesssim \varepsilon_1$ , the distinct feature of the system patterns is the existence of a giant cluster. Due to this special feature, we call these states the giant-cluster state.

Besides the giant cluster, we are also interested in the properties of the small clusters. We plot in Fig. 5(c) the distribution of  $n_c$  and in Fig. 5(d) the size distribution of the small clusters  $L_i$  that surround the giant cluster in the pattern. As shown in Fig. 5(c), the distribution of  $n_c$  follows a power-law

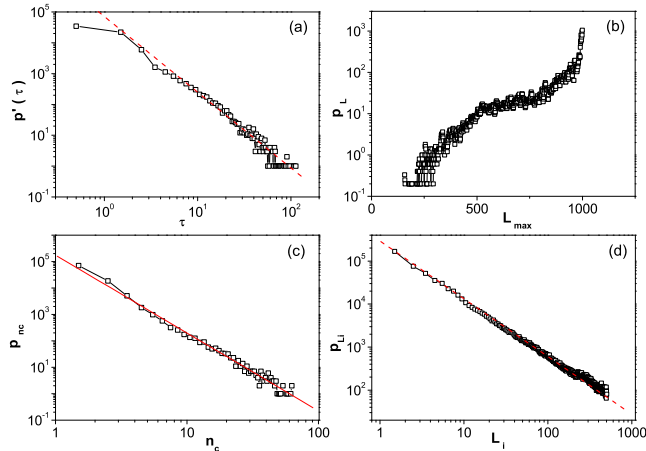


FIG. 5: (Color online) Statistical properties of the on-off intermittency plotted in Fig. 4. (a) The power-law scaling of the laminar-phase distribution of  $n_c$ . The fitted slope is about  $-2.3 \pm 0.05$ . (b) The size distribution of the size of the giant cluster. (c) The power-law distribution of the number of small clusters  $n_c$ . The fitted slope is about  $-3 \pm 0.1$ . (d) The power-law scaling on the size distribution of the small clusters. The fitted slope is about  $-1.2 \pm 0.01$ .

scaling with the fixed exponent is about  $\gamma \approx -3 \pm 0.05$ . The heterogeneous distribution of  $n_c$  indicates that, in the giant-cluster state, the system is usually broken into only a few number of clusters. An interesting finding exists in the size distribution of the small clusters. As shown in Fig. 5(d), in range  $L_i \in [1, N/2]$  a power-law scaling is found between  $P_{L_i}$  and  $L_i$ , with the fitted exponent is about  $\gamma \approx -1.1 \pm 0.05$ . The distribution of  $L_i$  confirms the finding of Fig. 5(c) that the small clusters which join or separate from the giant cluster are usually of small size.

Combining the findings of Fig. 4 and Fig. 5, the picture of pattern evolution in the bifurcation region  $\varepsilon \lesssim \varepsilon_1$  now becomes clear. Generally speaking, the evolution can be divided into two opposite dynamical processes happening around the giant cluster: the separation and integration of the small clusters. During the separation process, the small clusters are escaped from the giant cluster, which weakens the dominant role of the giant cluster and makes the pattern complicated. However, the separated clusters occupy only a small proportion of the nodes [Fig. 5(c)], the majority nodes are still attached to the giant cluster, which sustains the synchronization skeleton and keeps the system on the high coherence states. At some rare moments the giant cluster may disappears, and the pattern is composed by only small clusters of  $L_i < N/2$ . At these moments, the synchronization skeleton is broken, the pattern becomes even complicated and the system coherence reaches its minimum. In contrast, during the process of cluster integration, the giant cluster will increase its size by attracting the small clusters, and gradually towards the state of global synchronization. It should be noticed that the separation and integration processes are uneven and are typically occurring at the same time. For instance, during the separation process, while the system evolution is dominated by the separation of

new small clusters from the giant cluster, there could be some small clusters rejoin to the giant cluster.

### C. Pattern evolution of the scattering-cluster state

As we further decrease the coupling strength from  $\varepsilon_1$ , the picture of pattern evolution will be totally changed. With  $\varepsilon = 0.79$ , we plot in Fig. 6 the same statistics as in Fig. 5. The first observation is the loss of the global synchronization state, as can be found from the time variation of  $n_c$  plotted in Fig. 6(a). The loss of global synchronization becomes even clear if we compare Fig. 6(a) with Fig. 4(a): in Fig. 6(a), except the moment at  $t = 0$ , the system can never reach the synchronization state at  $n_c = 1$  and very often it is broken into a large number of small clusters at about  $n_c \sim 10^2$ . The fact that the pattern is decomposed into a large number of small clusters is also manifested by the distribution of  $n_c$ , as plotted in Fig. 6(b). Instead of the power-law distribution found in the giant-cluster state, in the scattering-cluster state  $n_c$  follows a Gaussian distribution [Fig. 6(b)]. As  $\varepsilon$  further decreases from  $\varepsilon_1$ , the mean value of  $n_c$  will shift to the larger values, as indicated by the  $\varepsilon = 0.78$  curve plotted in Fig. 6(b). The second observation is the disappearance of the giant cluster. As shown in Fig. 6(c), the size distribution of the largest cluster also follows a Gaussian distribution, with its mean value locates at  $\langle L_{\max} \rangle < N/2$ . The distribution of Fig. 6(c) is very different to that of Fig. 5(b), where in Fig. 5(b) the largest (giant) cluster has size  $L_{\max} \approx N$  in most of the time. As  $\varepsilon$  decreases, the mean value of the largest cluster  $\langle L_{\max} \rangle$  will shift to small values and the variance of  $L_{\max}$  will be decreased, as indicated by the  $\varepsilon = 0.78$  curve plotted in Fig. 6(c). Similar to plot of Fig. 5(d), we have also investigated the distribution of  $L_i$ , the sizes for all the small clusters appeared in the system evolution [Fig. 6(d)]. It is found that the distribution of  $L_i$  follows a power-law distribution for  $L_i < N/2$ , while having an exponential tail for  $L_i > N/2$ . Numerically we find that the exponent of the power-law section, i.e. in range  $L_i \in [1, 200)$ , is about  $-2 \pm 0.05$ , while the fitted exponent for the exponential section is about  $-4.5 \times 10^{-3} \pm 2 \times 10^{-5}$ . These two exponents, however, are changing with  $\varepsilon$ . As  $\varepsilon$  decreases, the two exponents will shift to some small values.

Combining Fig. 5 and Fig. 6, we are able to outline the transition process of network synchronization nearby the bifurcation points, i.e., the transition from the giant-cluster state to the scattering-cluster state as  $\varepsilon$  leaves away from  $\varepsilon_1$ . In the region of  $\varepsilon \lesssim \varepsilon_1$ , the pattern is composed by a giant cluster and a few number of small clusters, i.e. the giant-cluster state. As  $\varepsilon$  decreases from  $\varepsilon_1$  gradually, more and more small clusters will be emitted out from the giant cluster and, as a consequence, both the size of the giant cluster and the fraction of synchronization time will be decreased. Then, at about  $\varepsilon_c \approx 0.832$ , the giant cluster disappears and the pattern of the system is composed by several larger clusters, of size  $L_{\max} \lesssim N/2$ , together with many small clusters of heterogeneous size distribution, i.e. the scattering-cluster state. After that, as  $\varepsilon$  decreases from  $\varepsilon_c$ , the clusters shrink their size by breaking into even small clusters, and the pat-

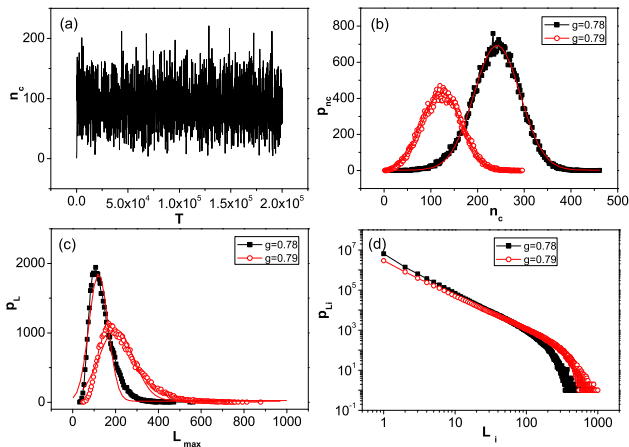


FIG. 6: (Color online) The dynamical and statistical properties of pattern evolution for  $\varepsilon = 0.79$ . (a) The time evolution of  $n_c$ . (b) The Gaussian distribution of the number of the small clusters  $n_c$ . (c) The Gaussian distribution of the size of the largest cluster  $L_{\max}$ . (d) The two-segment distribution on the size of the small clusters  $L_i$ . In the region of  $L_i < 200$ ,  $L_i$  follows a power-law distribution with fitted exponent is about  $-2 \pm 0.05$ ; while for  $L_i > 200$ , the distribution is exponential with the fitted exponent is about  $-4.5 \times 10^{-3} \pm 2 \times 10^{-5}$ . As  $\varepsilon$  further decreases from  $\varepsilon_1$ , the largest cluster becomes even smaller and more small clusters are emitted out from it. As illustrated by the  $\varepsilon = 0.78$  curves plotted in (b), (c) and (d).

tern becomes even complicated. The detail transition from the giant-cluster state to the scattering-cluster state is presented in Fig. 7, where the average number of clusters that the system is broken into  $\langle n_c \rangle$ , Fig. 7(a), and the average size of the largest cluster  $\langle L_{\max} \rangle$ , Fig. 7(b), are plotted as a function of the coupling strength in the LW bifurcation region. The transition is found to be smooth and steady, just as we have expected. Besides the giant cluster, another difference between the giant-cluster and scattering-cluster states exists in their pattern evolutions. In the giant-cluster state, while the configuration of the giant cluster is continuously updated by emitting or absorbing the small clusters, its main contents are stable and do not change with time. In contrast, in the scattering-cluster state the small clusters integrate with or separate from each other in a random fashion. Although occasionally there could be some large clusters show up in the pattern of the scattering-cluster state [Fig. 6(d)], these "large" clusters, however, are very fragile and will break into small clusters again in a short time. This quick-dissolving property stops the scattering-cluster state from having a high coherence.

## VI. CHARACTERIZING THE ACTIVE NODES

In the giant-cluster state, most of the nodes are organized into the giant cluster while few nodes, either in forms of small group or isolated node, are separating from or joining to the giant cluster with a high frequency. These active nodes, al-

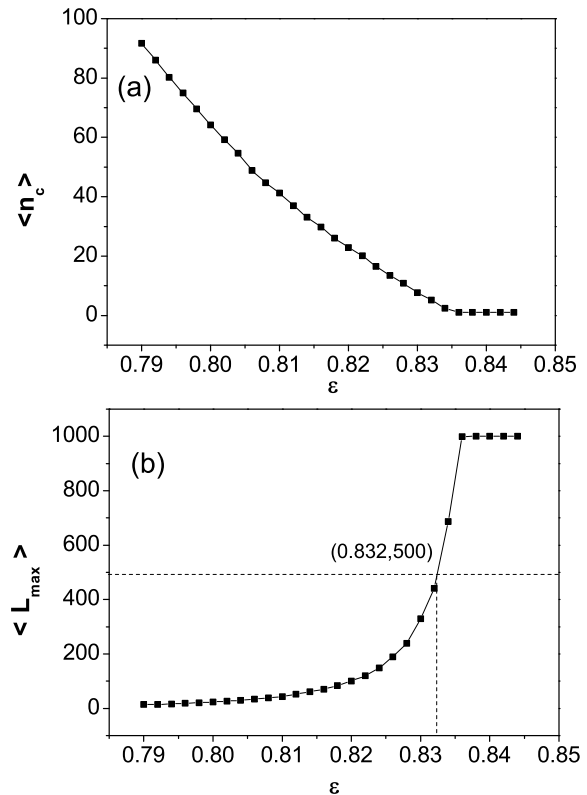


FIG. 7: The transition process of the network synchronization nearby the LW bifurcation point  $\varepsilon_1$ . (a) The average number of clusters that the system is broken into as a function of coupling strength. (b) The average size of the largest cluster as a function of coupling strength. Each date is an averaged result over  $10^8$  time steps.

though are few in amount, play an important role in network synchronization. Clearly, a proper characterization of these nodes will deepen our understandings on the system dynamics and give indications to the improvement of network performance. For instance, to improve the synchronizability of the system, we may either remove the few most active nodes from the network, or update their coupling strengths specifically.

In characterizing the active nodes, the following properties are of general interest: 1) what's the dependence of the node activity on the network topology? can we characterize these nodes by the known network properties such as node degree or betweenness? 2) are their locations sensitive to the coupling strength? and 3) what's the effect of bifurcation type on their locations? In the following we will explore these questions by numerical simulations.

We first try to characterize the active nodes by their topological properties. For the giant-cluster state described in Fig. 4, we plot in Fig. 8(a) the probability  $p_{u1}$  that each node stays in the giant cluster. While the majority nodes stay in the giant cluster with a high probability  $p_{u1} \approx 1$ , few nodes are of unusually small probabilities: 1 percent of the nodes have  $p_{u1} < 0.8$ . One important observation of Fig. 8(a) is that the locations of the active nodes are entangled with those of



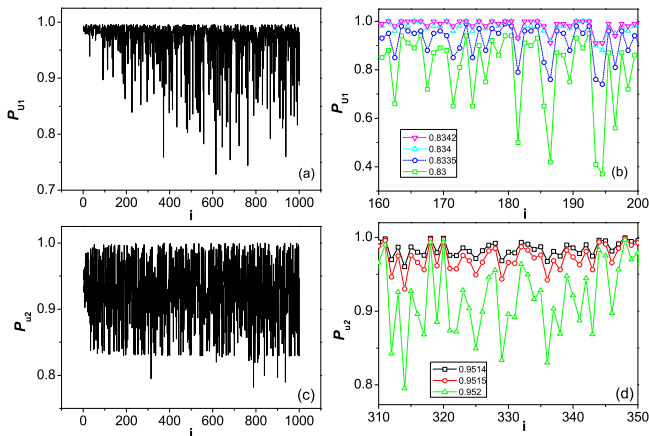


FIG. 8: (Color online) The properties of the active nodes. (a) For the giant-cluster state shown in Fig. 4, the probability that node stays in the giant cluster versus the node index. (b) A segment of (a) but with different coupling strengths nearby the LW bifurcation point  $\varepsilon_1$ . (c) For the giant-cluster state ( $\varepsilon = 0.952$ ) nearby the SW bifurcation point, the probability that node stays in the giant cluster versus the node index. (d) A segment of (c) under different coupling strengths nearby the SW bifurcation point  $\varepsilon_2$ .

the stable nodes. Noticing that in the BA growth model node of higher index in general assume the smaller degree, the observation of Fig. 8(a) therefore indicates the independence of the node degree to the node stability, or the inaccuracy of using degree to characterize the node activity. Specifically, in Fig. 8(a) the 5 most unstable nodes, by a descending order of  $p_{u1}$ , are those of degrees  $k = 47, 36, 26, 10, 4$ , respectively. Except the one of  $k = 4$ , all the other nodes have higher degrees. Another well-known topological property of complex network is the node betweenness, which counts the number of shortest paths that pass through each node and actually evaluates the node importance from the global-network point of view. This global-network property, however, is also incapable to characterize the active nodes. In Tab. 1 we list the detail information about the 5 most active nodes in Fig. 8(a), where the inaccuracy of node degree or node betweenness in characterizing the active nodes are summarized.

TABLE I: For the attaching probability  $p_i$  plotted in Fig. 8(a), we list the 5 most unstable nodes and try to characterize them by a set of topological quantities including the node index  $i$ , the attaching probability  $p_i$ , the stability rank  $p_i$ -rank, the node degree  $k_i$ , the degree rank  $k_i$ -rank, the node betweenness  $B_i$ , and the betweenness rank  $B_i$ -rank.

Node index $i$	$p_i$	$p_i$ -rank	$k_i$	$k_i$ -rank	$B_i$	$B_i$ -rank
615	0.72797	1	5	39→537	1301	280
762	0.74424	2	5	39→537	1375	356
680	0.75416	3	4	1→338	1254	680
372	0.7591	4	6	538→645	1440	406
938	0.75972	5	4	1→338	1215	159

We go on to investigate the affection of the coupling strength on the locations of the active nodes. In Fig. 8(b) we fix the network topology and compare the node activities under different coupling strengths nearby the bifurcation point  $\varepsilon_1$ . It is found that, despite of the changes in  $p_{u1}$ , the locations of the active nodes are kept unchanged. That is, the active nodes are always the first ones to escape from the giant cluster whenever the network is unsynchronizable. We have also investigated the affection of the bifurcation type on the locations of the active nodes. By choosing the coupling strength nearby the SW bifurcation  $\varepsilon = 0.952 \gtrsim \varepsilon_2$ , we plot in Fig. 8(c) the node attaching probability  $p_{u2}$  as a function of the node index  $i$ . An interesting finding is that, comparing to the situation of LW bifurcation [Fig. 8(a)], the locations of the active nodes have been totally changed in Fig. (c). In Tab. 2 we list the detail information about the 5 most active nodes in Fig. 8(c), again their locations can not be predicted by the node degree or betweenness. Similar to the LW bifurcation, the locations of the active nodes are also independent to the coupling strength at the SW bifurcation, as shown in Fig. 8(d).

TABLE II: Similar to Tab. I but for the attaching probability  $p_i$  plotted in Fig. 8(c). Comparing to Tab. I, one important observation is the changed locations of the active nodes due to the changed bifurcation type.

Node index $i$	$p_i$	$p_i$ -rank	$k_i$	$k_i$ -rank	$B_i$	$B_i$ -rank
43	0.78196	1	9	779→813	2847	813
35	0.78969	2	18	936→940	8513	953
714	0.795	3	4	1→338	1215	158
130	0.79652	4	13	886→901	4200	886
154	0.19944	5	10	814→846	2898	815

Previous studies about network synchronization have shown that, while individually it is difficult to predict the dynamical behavior of each node, the average performance of an ensemble of nodes of the same network properties do have some reliable characters. For instance, it has been shown that in complex networks the high-degree nodes are on average more synchronizable than the low-degree ones [19]. Regarding to the problem of node activities, it is natural to ask the similar question: are the high-degree nodes more synchronized than the low-degree nodes? In Fig. 9 we plot the average attaching probability  $\langle p_{u1} \rangle_k$  as a function of degree  $k$ . Still, we can not find a clear dependence of  $\langle p_{u1} \rangle_k$  on  $k$ .

## VII. DISCUSSIONS AND CONCLUSION

It is worthy of note that our studies of active nodes are only focused on the giant-cluster state, and the purpose is to understand their dynamics and reveal their properties. By ensemble

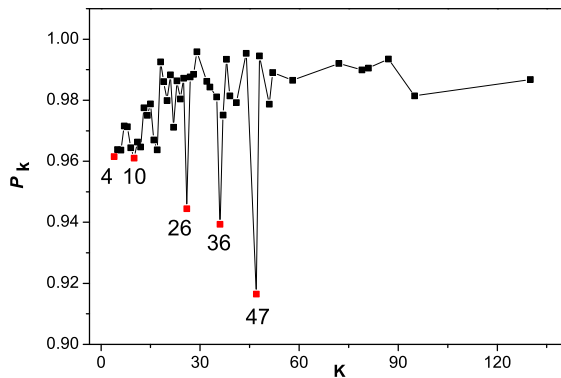


FIG. 9: (Color online) The average attaching probability  $\langle p_{u1} \rangle_k$  as a function of node degree  $k$ . On average, the 5 most unstable nodes are those of degrees  $k = 47, 36, 26, 10, 4$ . Still, we can not find a clear dependence between  $\langle p_{u1} \rangle_k$  and  $k$ .

average, we may be able to improve our prediction of the active nodes, say for example the dependence of  $\langle p_{u1} \rangle_k$  on  $k$  in Fig. 9 may be smoothed if we average the results over a large number of network realizations. Such an improvement, however, comes at the cost of the decreased prediction accuracy due to the increased candidates. Taking Fig. 9 as an example, although it is noticed that nodes of  $k = 4$  in general are more active than those of other degrees, only one of them is listed as the 5 most unstable nodes [Tab. 1]. In specific, among the total number of 338 nodes which have degree  $k = 4$ , most of them are tightly attracted to the giant cluster (90 percent of them have attaching probabilities  $p_{u1} > 0.95$ ). Therefore, in terms of precise prediction, the average method is infeasible in practice.

Beside node degree and betweenness, we have also checked the dependence of the property of node activity to some other well-known network properties such as the clustering coefficient, the modularity, and the assortativity. However, none of them is suitable to characterize the active nodes, their performance is very similar to that of the node degree described in Tab. 1 and Tab. 2. Our study thus suggests that, to give a precise prediction to the active nodes, we may need to develop some new quantities.

Despite of the amount of studies carried on network synchronization, to the best of our knowledge, we are the first to study the nonstationary pattern in unsynchronizable complex

networks. In Ref. [9] the authors have discussed the transient process of global synchronization in complex networks, but their study are concentrating on the synchronizable state in which, during the course of system evolution, small clusters integrate into larger clusters monotonically and finally reach the synchronization state. After that, the system will always stay on the synchronization state. Our works are also different to the studies of Refs. [10, 20]. Similar to our works, in these studies the authors also consider the problem of pattern formation in unsynchronizable networks, but their interests are focused on the *stationary pattern* of the system. That is, the size and contents of the clusters do not change with time. In contrast, in our studies both the size and contents of the clusters are variable.

In summary, we have reported and investigated a kind of new phenomena in network synchronization: the nonstationary pattern. That is, the final state of the network settles neither to the synchronization state nor to any stationary state of fixed pattern, the system is travelling among all the possible patterns in an intermittent fashion (the pattern can be of any configuration, but its probability of showing up is pattern-dependent). We attribute this nonstationarity to the asymmetric topology of the complex networks, and its dynamical origin can be understood from the property of the finite-time Lyapunov exponent associated to the desynchronized mode. Two types of synchronization formats, the complete synchronization and the temporal phase synchronization, have been employed to detect the nonstationary dynamics. For coupling strength immediately out of the stable region, the pattern evolution is characterized by the process of on-off intermittency and the existence of the giant-cluster; while if the coupling strength is far away from the bifurcation points, the pattern evolution is signatored by the random interactivities among the number of small clusters. A remarkable finding is that, in the giant-cluster state the locations of the active nodes are independent of the coupling strength but are sensitive to the bifurcation types. The active nodes, however, can not be characterized by the currently known network properties, further investigations about their identification are necessary. While we are hoping our studies about nonstationary pattern could give some new understandings to the dynamics of coupled complex systems, we also hope that our findings about unsynchronizable networks could be used to some practical problems where system maintains their normal functions only under the unsynchronizable states, for example the problem of epileptic seizures [21].

- 
- [1] D.J. Watts and S.H. Strogatz, Nature **393**, 440 (1998); A.-L. Barabási and R. Albert, Science **286**, 509 (1999); R. Albert and A.-L. Barabási, Rev. Mod. Phys. **74**, 47 (2002).  
 [2] S. Boccaletti and L.M. Pecora, Chaos **16**, 015101 (2006); A. E. Motter, M. A. Matías, J. Kurths, E. Ott, Physica D **224**, 7 (2006); S. Boccaletti, V. Latora, Y. Moreno, M. Chavez, and D.-U. Hwang, Phys. Rep. **424**, 175 (2006).  
 [3] X.F. Wang and G. Chen, Int. J. Bifurcation Chaos Appl. Sci.

- Eng. **12**, 187 (2002).  
 [4] T. Nishikawa, A. E. Motter, Y.-C. Lai, and F. C. Hoppensteadt, Phys. Rev. Lett. **91**, 014101 (2003).  
 [5] A.E. Motter, C. Zhou, and J. Kurths, Europophys. Lett. **69**, 334 (2005); Phys. Rev. E **71**, 016116 (2005); AIP Conf. Proc. **776**, 201 (2005); C. Zhou, A.E. Motter, and J. Kurths, Phys. Rev. Lett. **96**, 034101 (2006).  
 [6] M. Chavez, D.-U. Hwang, A. Amann, H.G.E. Hentschel, and S.

- Boccaletti, Phys. Rev. Lett. **94**, 218701 (2005); D.-U. Hwang, M. Chavez, A. Amann, and S. Boccaletti, Phys. Rev. Lett. **94**, 138701 (2005).
- [7] L.M. Pecora and T.L. Carroll, Phys. Rev. Lett. **80**, 2109 (1998); M. Barahona and L. M. Pecora, *ibid.*, **89**, 054101 (2002).
- [8] D.-S. Lee, Phys. Rev. E **72**, 026208 (2005); J. Gómez-Gardeñes, Y. Moreno, and A. Arenas, Phys. Rev. Lett. **98**, 034101 (2007).
- [9] A. Arenas, A. Díaz-Guilera, and C. J. Pérez-Vicente, Phys. Rev. Lett. **96**, 114102 (2006); C. Zhou, L. Zemanová, G. Zamora, C. C. Hilgetag, and J. Kurths, *ibid.*, **97**, 238103 (2006)
- [10] S. Boccaletti, M. Ivancheko, V. Latora, A. Pluchino, and A. Rapisarda, Preprint physics/0607179 (2006).
- [11] M. Zhan, Z.G. Zheng, G. Hu, and X.H. Peng, Phys. Rev. E **62**, 3552 (2000); Y. Zhang, G. Hu, H.A. Cerdeira, S. Chen, T. Braun, and Y. Yao, Phys. Rev. E **63**, 026211 (2001); B. Ao and Z. Zheng, Europhys. Lett. **74**, 229 (2006); X. Zhang, M. Fu, J. Xiao, and G. Hu, Phys. Rev. E **74**, 015202 (2006).
- [12] E. Ott and J.C. Sommerer, Phys. Lett. A **188**, 39 (1994); M. Ding and W. Yang, Phys. Rev. E **56**, 4009 (1997); S.H. Wang, J. Xiao, X.G. Wang, B. Hu, and G. Hu, Eur. Phys. J. B **30**, 571 (2002); J.G. Restrepo, E. Ott, and B. Hunt, Phys. Rev. Lett. **93**, 114101 (2004).
- [13] X.G. Wang, Y.-C. Lai, and C.-H. Lai, Preprint nlin.CD/0608035 (2006).
- [14] L. A. Bunimovich, A. Lambert, and R. Lima, J. Stat. Phys. **65**, 253 (1990); J.F. Heagy, T.L. Carroll, and L.M. Pecora, Phys. Rev. Lett. **73**, 3528 (1994); *ibid.*, **74**, 4185 (1995).
- [15] M.A. Matias, V.P. Munuzuri, M.N. Lorenzo, I.P. Marino, and V.P. Villar, Phys. Rev. Lett. **78**, 219 (1997); G. Hu, J. Yang, and W. Liu, Phys. Rev. E **58**, 4440 (1998).
- [16] A. Pikovsky and U. Feudel, Chaos **5**, 253 (1995); X. Wang, M. Zhan, C. H. Lai, and Y.-C. Lai, Phys. Rev. Lett. **92**, 074102 (2004).
- [17] N. Platt, E.A. Spiegel, and C. Tresser, Phys. Rev. Lett. **70**, 279 (1993); E. Ott and J. C. Sommerer, Phys. Lett. A **188**, 39 (1994); Y. Nagai and Y.-C. Lai, Phys. Rev. E **55**, 1251 (1997).
- [18] A.S. Pikovsky, M.G. Rosenblum, and J. Kurths, *Synchronization: A Universal Concept in Nonlinear Science* (Cambridge University Press, Cambridge, UK, 2001); S. Strogatz, *Sync: The Emerging Science of Spontaneous Order* (Hyperion, New York, 2003).
- [19] C. Zhou and J. Kurths, Chaos **16**, 015104 (2006).
- [20] S. Jalan, R.E. Amritkar, and C.-K. Hu, Phys. Rev. E **72**, 016211 (2005); *ibid.*, **72**, 016212 (2005).
- [21] Y.-C. Lai, M. G. Frei, I. Osorio, and L. Huang, Phys. Rev. Lett. **92**, 108102 (2007).